Chemical Engineering Science 116 (2014) 161–171

Contents lists available at ScienceDirect

Chemical Engineering Science

journal homepage: www.elsevier.com/locate/ces

Multi-scale flow simulation of automotive catalytic converters

Cansu Ozhan, Daniel Fuster*, Patrick Da Costa

CNRS (UMR 7190), Université Pierre et Marie Curie, Institut Jean le Rond d'Alembert, 4 place Jussieu, 75252, Paris Cedex 05, France

HIGHLIGHTS

- We model the flow occurring at multiple scales inside catalytic converters.
- A subgrid model is proposed for the flow in the monolith channels.
- Adaptive Mesh Refinement techniques are optimized to capture the main flow features.
- The new model is validated against the experimental results reported by Benjamin.
- The new model allows for significant computational time savings compared to the full simulation.

ARTICLE INFO

Article history:
Received 3 December 2013
Received in revised form
24 March 2014
Accepted 30 April 2014
Available online 14 May 2014

Keywords:
Catalytic converters
Computational fluid dynamics
Adaptive mesh refinement
Flow mal-distribution

ABSTRACT

The flow distribution within the automotive catalytic converter is an important controlling factor on the overall conversion efficiency. Capturing the flow features minimizing the computational cost is the first important step towards the solution of the complex full engineering problem. In this work we present a novel approach that combines physical and numerical multi-resolution techniques in order to correctly capture the flow features inside an automotive catalytic converter. While Adaptive Mesh Refinement techniques are optimized in order to minimize the computational effort in the divergent region, a novel subgrid model is developed to describe the flow inside the catalytic substrate placed between the convergent and divergent regions. The proposed Adaptive Mesh Refinement methods are tested for two test cases representative of the flow features found in the divergent region of a catalytic converter. The performance of the new subgrid model is validated against the non-uniformity index and the radial velocity profile data obtained by Benjamin et al. (2002). The effective coupling of AMR techniques and the subgrid model significantly reduces the error of the numerical predictions to 5–15% in conditions where the full simulation of the problem is out of current computational capabilities.

1. Introduction

Transportation is responsible for a large part of global emissions (Pachauri and Reisinger, 2007). This problematic has led to governments to establish very stringent conditions for the maximum emissions levels. Post-treatment systems need to be further developed in order to meet with these emissions requirements. A large part of the current studies is devoted to find efficient catalysts to improve the reaction efficiency, but one can also optimize the performance of these equipments by acting on the flow distribution inside the catalytic converter. A few studies (Agrawal et al., 2012; Bella et al., 1991; Guojiang and Song, 2005; Karvounis and Assanis, 1993) have focused on the flow distribution effect on the conversion efficiency. However, the interaction between flow and conversion efficiency has not yet been understood completely.

In an ideal situation, the flow at the converter inlet is uniform. However, in practical cases, high Reynolds numbers, pulsating flow, abrupt expansion, and the impact of porous media lead to non-homogeneous and non-uniform velocity profiles at the inlet converter. Because the velocity profile is non-uniform, we find different inlet velocities (hence different mass flow rates) in the substrate monolith channels. This results in premature degradation of the catalyst in areas of high flow rates and poor volume utilization of catalyst in areas of low flow rates, which turns into a decrease of the system's efficiency (Benjamin et al., 2002; Karvounis and Assanis, 1993). The flow inside the system under these physical and geometrical effects generates large range of scales on the flow in addition to the molecular scales inherent of the chemical reactions that occur inside the catalytic medium. Capturing all the physics and chemistry inside the system is out of reach for the available computational capabilities (Nien et al., 2013; Siemund et al., 1996).

The development of numerical tools and models is crucial in order to optimize the performance of catalytic converters

* Corresponding author.
E-mail address: fuster@dalembert.upmc.fr (D. Fuster).

http://dx.doi.org/10.1016/j.ces.2014.04.044
0009-2509/

(Chatterjee et al., 2002; Tischer et al., 2001; Tischer and Deutschmann, 2005). Modeling approaches for automotive catalytic converters have presented by Pontikakis et al. (2004). These tools must be capable of predicting the effect of externally controlled variables in the flow distribution. The simulation of the entire system is not simple due to all the complex transport and chemical phenomena that take place inside the system. Thus, the large range of lengthscales involved in the process makes the full solution of the basic equations far beyond current available computational capabilities. As an alternative, we can resort to reliable models and specific multi-resolution techniques in order to investigate the process (Charpentier, 2005). These models aim at providing a better understanding of the system's response to externally controlled variables (e.g. inlet velocities, effect of geometry, etc.) keeping a low computational cost.

In this work we develop and test multi-resolution numerical techniques and models to capture the main physical process taking place inside automotive catalyst systems. In particular we focus this work on the development of numerical techniques and models to correctly capture the characteristics of the flow created inside these systems in order to establish a solid base on which implement chemical reaction models. We propose a subgrid model for the flow inside the catalytic substrate which is coupled with the full solution of the Navier–Stokes equations in the diffuser and convergent regions, where Adaptative Mesh Refinement (AMR) techniques are optimized to minimize the computational cost. A free CFD package (Gerris) is used as a platform to implement the models (Popinet, 2003, 2009).

Adaptative Mesh Refinement is a numerical technique to concentrate the computational effort on regions where the flow properties vary dramatically, coarsening the regions where the flow properties variations are small (Hauke et al., 2008; Popinet, 2003). These techniques have been already shown significant computational time savings in problems involving liquid atomization (Fuster et al., 2009b, 2013) and other multiphase flow studies (Fuster et al., 2009a). In this work we investigate the capability of AMR to reduce the computational limitations related to the Direct Numerical Simulation (DNS) of turbulent flows typically found inside catalytic converter systems. Various authors have tried to explore the capabilities of AMR techniques for the particular problem of turbulent flow simulations (Bockhorn et al., 2009; Gao and Groth, 2006, 2010; Nazarov and Hoffman, 2013). Some of these methods, despite their accuracy, suffer of being exceedingly computationally expensive which impedes their application to real problems. This fact strengthens the compromise that one has to reach between accuracy and computational effort. Turbulent simulations usually have related long simulation runs in order to obtain reproducible statistics of the flow of interest. Thus, in this work we focus on AMR techniques whose computational cost is negligible compared to the cost related to the numerical solution of the flow equations.

In this study, the general problem is presented first, then the derivation of a simplified model for the flow in catalytic substrate is developed. The accuracy of the model is demonstrated by comparing the results with the full simulation of the flow in this region. Then, we focus our efforts in deriving efficient Adaptive Mesh Refinement methods for the flow characteristics typically found in the divergent region (e.g. recirculation regions and shear layer). The accuracy and efficiency of the method is verified against related test cases with analytical solution. The new model is validated against the experimental data reported by Benjamin et al. (2002). Finally, we present a full numerical example of a typical automotive catalyst system.

2. Problem formulation

A typical and ideal automotive catalytic converter systems consist of an inlet pipe, a diffuser, a monolithic substrate, an outlet nozzle and an outlet pipe. The monolithic substrate is either ceramic or metallic and coated with aluminium washcoat which supports the noble metals (catalysts). The monolith comprises numerous parallel narrow channels (of the order of 1 mm) to increase the surface area where reactions occur. In after-treatment systems, different flow patterns are present due to changes in the cross section from the diffuser inlet to the nozzle outlet.

Fig. 1 depicts a classical example of the flow features found inside the system. In the inlet diffuser the flow expands and becomes turbulent (Neve, 1993; Shuja and Habib, 1996; Ubertini and Desideri, 2000). At the entrance of expansion a turbulent free shear layer develops. A main flow jet region appears close to the axis of symmetry whereas a recirculation flow region appears right after the beginning of the expansion. The intense recirculation induces high energy dissipation rates within the separated flow region (Forrester and Evans, 1997). The flow within the catalytic channel is significantly simpler. The flow is laminarized by viscous forces inside the narrow channels that induce a significant pressure drop across the channel compared to inlet diffuser and outlet nozzle. The characteristic Reynolds numbers in this region do not exceed 500 (Karvounis and Assanis, 1993). Finally, at the outlet nozzle, the section contracts and we find swirl flow (Forrester and Evans, 1997).

In the next subsections, the governing equations and models to solve these equations are discussed in detail.

3. Governing equations

3.1. Full model

The incompressible fluid assumption is widely used in the literature for the simulation of the flow in catalytic converters (Chakravarthy et al., 2003; Guojiang and Song, 2005; Holmgren et al., 1997; Lai et al., 1992). Treating the exhaust gas as incompressible fluid is a reasonable approximation since the Mach number is smaller than 0.05, acoustic waves have a negligible impact (Chakravarthy et al., 2003) and the variations in pressure are less than 10% of the absolute pressure (Holmgren et al., 1997).

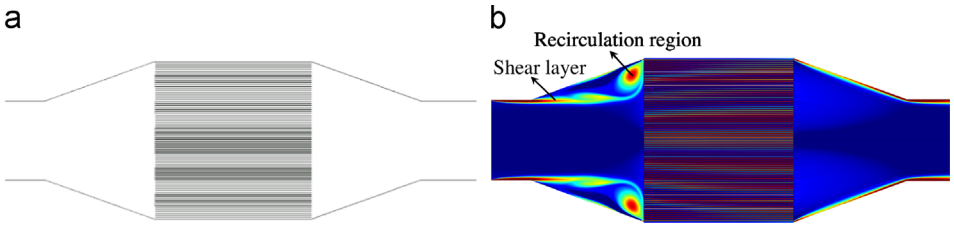

Fig. 1. Catalytic converter. Typical flow patterns inside a catalytic converter (Re = 10,000) in the symmetric plane. A shear layer and a large recirculation region are observed in the diffuser region. The flow is re-laminarized inside the catalytic channels.

For the sake of simplicity, we assume that the temperature change in the system is not significant and hence the fluid properties are constant. Under these assumptions and considering the gas as a Newtonian fluid, the governing equations for the flow are

$$\nabla \cdot \mathbf{u} = 0, \tag{1}$$

$$\rho\left(\frac{\partial \mathbf{u}}{\partial t} + \mathbf{u} \cdot \nabla \mathbf{u}\right) = -\nabla p + \mu \nabla^2 \mathbf{u} + S. \tag{2}$$

where t is the time, $\mathbf{u}$ is the velocity, ρ is the fluid density, p is the pressure, μ is the viscosity and S is a momentum source term.

In addition, when chemical reactions inside the system need to be modeled, we have to add N transport equations, being N the number of components present in the system. For the ith component we write

$$\frac{\partial c_i}{\partial t} = \nabla \cdot (D \nabla c_i) - \nabla \cdot (\mathbf{u} c_i) + R_i \tag{3}$$

where c_i is the concentration of the ith component, D is the diffusion coefficient and R_i is the reaction rate.

These equations can be solved by imposing proper boundary conditions. Typically we assume that the velocity at the inlet is known and we apply a classical outflow boundary condition at the outlet section (Dirichlet boundary condition for pressure and Neumann boundary condition for the normal velocity). The velocity at the solid walls is imposed equal to zero.

As stated above, the full solution of these equations is exceedingly expensive and we need to propose simplified solution strategies that we apply in regions where the flow features are already well captured by simple models. In particular, the flow inside the catalytic converter is a good candidate for such models. In the next subsection, we present the approach considered to model the flow in this region and how the model is coupled to the full numerical solution of the Navier–Stokes in the diffuser and convergent regions.

3.2. Subgrid models

3.2.1. Pressure drop model for monolithic channels

The flow inside monolithic channels is usually a fully developed laminar flow where the averaged velocity is kept constant by mass conservation. In these conditions, the pressure drop inside the channel is mainly induced by viscous forces and the flow is known to be well represented by the Hagen–Poiseuille pressure drop model (Heck et al., 2001)

$$\Delta p = \frac{32}{\mathrm{Re}_c}\frac{L}{d}\rho u^2, \tag{4}$$

where Re_c is the Reynolds number inside the channel defined with the channel diameter d and L is the channel length.

As expected, the full simulation of pipe flow for the range of Reynolds numbers typically found inside the catalytic channels fits well the theoretical result (Fig. 2). The numerical data of a pipe flow is consistent with the Hagen–Poiseuille model and we can therefore replace the flow inside the channels by a pressure jump model as follows. The catalytic region is replaced by an infinitesimal thin interface along which only transversal velocity is allowed and where the pressure jump is imposed. In the Navier–Stokes equations, this pressure jump can be imposed by adding a source term of the type,

$$\rho\left(\frac{\partial \mathbf{u}}{\partial t} + \mathbf{u} \cdot \nabla \mathbf{u}\right) = -\nabla p + \mu \nabla^2 \mathbf{u} + C(\mathbf{u})\delta_s \mathbf{n} \tag{5}$$

where δ_s is a Dirac delta function used to denote that the pressure jump is applied at the interface that represents now the catalytic converter (see Fig. 3), $\mathbf{n}$ is the normal to this interface and $C(\mathbf{u})$ is the function that imposes the desired pressure jump as a function of the velocity,

$$C(\mathbf{u}) = \frac{32}{\mathrm{Re}_c}\frac{L}{d}\rho\left(\frac{u}{A_O}\right)^2 \tag{6}$$

where A_O represents the open frontal area of the monolith substrate.

We remark that the subgrid model is naturally coupled with the full solution of the Navier–Stokes equations in the divergent and convergent region, where the source term is set to zero. The validation of the model is discussed in Section 5.

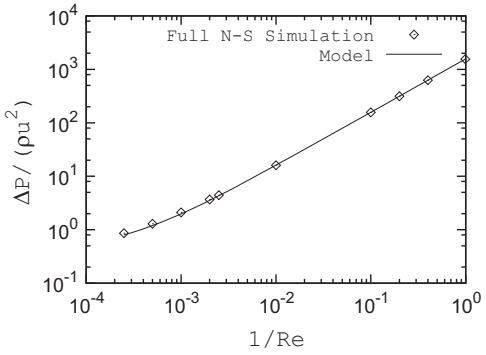

Fig. 2. Nondimensional pressure drop obtained by the full numerical solution of the Navier–Stokes equations as a function of the Reynolds number (◇) for a pipe geometry. For reference, the pressure drop predicted by the Hagen–Poiseuille pressure drop model is included (-).

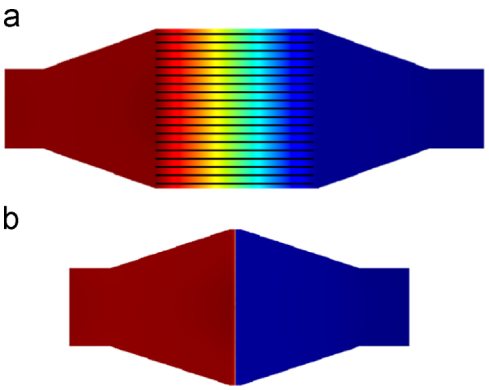

Fig. 3. Pressure distribution in the full geometry and reduced geometry proposed in this work. The catalytic converter is replaced by an interface where we apply a pressure jump as a function of the velocity according to the Hagen–Poiseuille pressure drop model. (a) Complete geometry and (b) reduced geometry.

3.2.2. Heterogeneous reaction model inside the catalytic converter

In the simulations included in this work we focus our analysis on the dynamics of the flow, neglecting the reaction mechanisms taking place inside the catalyst monolith. However, we note that it is possible to develop the model further to obtain an approximate prediction of the reaction rates. Replacing the catalytic converter by an infinitely thin interface implies that one needs to model also the global reaction rate that occurs inside the catalytic converter by a simplified source term that we need to plug into Eq. (3).

The calculation of a proper expression for the source term is specific to the problem considered and can be very involved for a general case. However, in a first approximation, if we assume that the influence of homogeneous reactions is negligible compared to heterogeneous reactions, it is possible to find solutions for limiting regimes. The controlling factor of the reaction regime is the temperature. When the catalyst is not sufficiently warm, the reaction taking place on the solid walls is slow and the conversion

rate is low. This is the so-called kinetic transfer regime. When the monolith substrate is sufficiently warm, the reactions occur very rapidly and the reaction process turns out to be controlled by mass transfer (Depcik and Loya, 2012).

Analytical solutions for the transport equation for situations involving heterogeneous reaction are less extended than in the case of homogeneous reactions. However, one can still develop models valid under limiting conditions. For instance, for the mass transfer regime, which is the predominant mode of operation (Benjamin et al., 2004), the reactant concentration is almost zero at the catalytic wall and we can simplify the full transport equation to a convective-diffusion equation with surface reaction boundary condition. The analytical solution of this system can be obtained using the method of variable separation (Skelland, 1974). Similar to the pressure jump model, given the solution of the concentration along the tube, it is straightforward to obtain the effective reaction rate applied on the cell containing the thin interface that reproduces the global reaction rate as a function of the inlet velocity. This model would give a first approximation of the reaction rates as a function of the radial system. A further extension of models accounting for chemical reactions and the coupling effects between energy transfer mechanisms, chemical reactions and volume generation inside the monolith channels are currently under investigation.

4. Numerical method

To solve for the system of equations given by Eqs. (1) and (2) we use the Gerris Flow solver (Popinet, 2009). This solver can be easily adapted to source terms of the form proposed in the previous section due to the similarities found with the pressure jump across gas/liquid interfaces when surface tension effects are present.

Another interesting characteristic of the solver is the capability to perform Adaptive Mesh Refinement (AMR) using quadtree (octree in 3D) meshes. By using AMR in the convergent and divergent regions we expect a significant gain on the computational time with respect to solvers with uniform grids. In the next subsection, we give further details about the use of AMR for the specific problem of catalytic converters as well as the two test cases used for the optimization of the mesh refinement strategies.

4.1. Multi-resolution AMR techniques

In this work we decided to use a Hessian error estimator based on the h-refinement algorithm. These methods basically consist in trying to obtain an estimation of the error contained in the numerical solution by subtracting the numerical solution obtained at two different resolution levels. Octree meshes are suitable for h-refinement methods because by construction it is simple and computationally efficient to travel up and down through the octree structure. Given a leaf cell with a level of refinement l, one can express the solution of second order accuracy around the cell centered coordinate $\mathbf{x}_c^l$ using the Taylor expansion as

$$f(\mathbf{x}) = \overline{f}(\mathbf{x}_c^l) + (\mathbf{x}-\mathbf{x}_c^l)\cdot(\nabla\overline{f})_{\mathbf{x}_c}^l + O((\mathbf{x}-\mathbf{x}_c^l)^2), \tag{7}$$

where we use an overbar to denote the discretized quantities. Typically, a-posteriori error estimation methods try to get an estimate of $O((\mathbf{x}-\mathbf{x}_c^l)^2)$ for every cell in the computational domain. For regular octree meshes of size h, the maximum of the error scales as $O(h^2)$. This error can be estimated using the Taylor expansion for the parent cell at the $l-1$ level and subtracting it from the Taylor expansions at l level at the leaf cell center. Thus one gets

$$0 = \overline{f}(\mathbf{x}_c^{l-1}) + (\mathbf{x}_c^l-\mathbf{x}_c^{l-1})\cdot(\nabla\overline{f})_{\mathbf{x}_c}^{l-1} - \overline{f}(\mathbf{x}_c^l) + O((\mathbf{x}_c^l-\mathbf{x}_c^{l-1})^2). \tag{8}$$

Using $\overline{f}_{int}^{\,l-1}(\mathbf{x}_c)$ to denote the linear interpolation of the solution at the $l-1$ level at a given location and using that, for octree structures, $\mathbf{x}_c^l-\mathbf{x}_c^{l-1}=h/2$ is always satisfied, we obtain the following estimation of the discretization error:

$$O\left(\frac{h^2}{4}\right) \approx \left|\overline{f}_{int}^{\,l-1}(\mathbf{x}_c^l) - \overline{f}(\mathbf{x}_c^l)\right|. \tag{9}$$

The error above can be interpreted as a measure of the error at the $l-1$ which can be corrected extrapolating the error at the l level taking into account the spatial order of the method used, α, so that,

$$\varepsilon = \|\overline{f}-f\|_{L_q} \approx \frac{\|\overline{f}^{\,l-1}-\overline{f}^{\,l}\|_{L_q}}{2^\alpha}. \tag{10}$$

In this paper, we denote with η_{hes-L_q} the error estimation measured in the L_q norm using this Hessian method approach,

$$\eta_{hes-L_q} \equiv \|\varepsilon_e\|_{L_q(\Omega)} = \|\overline{f}-f\|_{L_q(\Omega)} \tag{11}$$

For the simulations shown in this work we choose the L_1 norm.

The question about which quantity f provides optimal results remains open. Typically, previous works use the error on the primitive variables (e.g. velocity) to define criteria to adapt the grid, but other choices are possible. For instance, in this work we have chosen the error in the vorticity field ($\omega = (\partial_z u^r - \partial_r u^z)e_\theta$) as a criterion to adapt the grid. For two-dimensional simulations, vorticity is a conserved scalar quantity. To write the Navier–Stokes equations in terms of the equivalent vorticity equation has been shown some desirable numerical properties in terms of accuracy and speed (Davies and Carpenter, 2001). Recent formulations (Olshanskii and Rebholz, 2010) have proposed the use of Helicity, which is the corresponding invariant of Euler's equations in three dimensions, to derive efficient numerical schemes especially designed to capture turbulent structures. These works reveal that the use of vorticity (or helicity) is usually advisable when one wants to capture turbulent structures. Thus, we propose here the use of the residual of the vorticity field as a good candidate to minimize the numerical error introduced when discretizing the vortices appearing in the divergent region.

4.2. Test cases for adaptive mesh refinement

As mentioned previously, the two main flow patterns found in the expansion region of catalytic converters are a shear layer and a recirculation region. In order to validate the accuracy and the efficiency of the proposed AMR method for these flow patterns, we decide to use the following tests. The first test is the measure the energy dissipation by a Lamb–Oseen vortex. This vortex model is representative of the vortices existing in the recirculation region in the inlet diffuser. The second test is the growth of random noise perturbations in a shear velocity region. The AMR efficiency of this example is also relevant for catalytic converters due to the shear layers generated in the abrupt expansion in the diffuser region.

4.2.1. Lamb–Oseen vortex

This example represents a solution to the two-dimensional viscous Navier–Stokes equations where axial and radial velocities are zero. Setting the initial vorticity field with a known circulation Γ to $w(r,0)=\Gamma\delta(x)\delta(y)$ it is possible to obtain the analytical solution of the velocity temporal

evolution as (Meunier and Villermaux, 2003)

$$u_\theta = \frac{\Gamma}{2\pi r}\left[1-\exp\left(-\frac{r^2}{4\nu t}\right)\right]. \quad (12)$$

where ν is the kinematic viscosity and r and θ are respectively the radial and the azimuthal coordinates. A characteristic length for this problem can be obtained by setting the radial distance at which the velocity norm is maximal,

$$l_c = 2.2418\sqrt{\nu t_0}. \quad (13)$$

For the simulations contained in this section we choose $\nu t_0 = 0.5$ in order to define a characteristic length different from zero. In addition, we set the circulation equal to $\Gamma = 1$ in a square domain with nondimensional length $L/l_c = 600$ where we impose Neumman boundary conditions for the velocity at all boundaries.

The initial velocity field is initialized according to Eq. (12). Fig. 4 represents the theoretical azimuthal velocity profiles as a function of the radius for different times. We note that the theoretical solution extends to infinity. This fact introduces a certain error at the domain boundaries when setting the domain size to a finite distance. This error cannot be attributed to the discretization method and therefore, cannot be captured by the error estimator. To solve this problem, we decide to measure the efficiency of the error estimators in a circular region of radius $R_c/l_c = 100$.

Fig. 5 depicts a classical velocity field and the corresponding grid distribution for a given example. The grid is significantly refined at the domain center where the velocity variations are important. Near the boundaries, the mesh is coarsened which significantly decreases the number of unknowns to be solved in the discrete form of the equations.

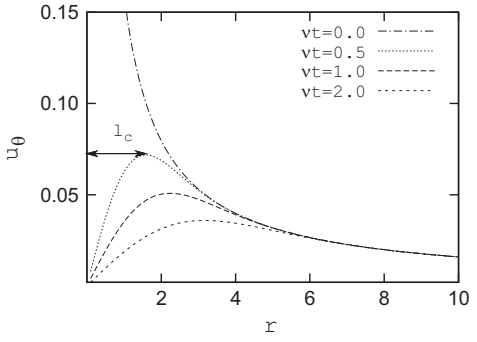

Fig. 4. Radial velocity norm distribution for various nondimensional times for Lamb–Oseen vortex test case.

Fig. 6 depicts the convergence curves obtained for a fixed grid and the AMR criteria, where an *effective* grid size is defined as $\Delta x = L/\sqrt{N_{\text{cells}}}$, N_{cells} being the total number of cells in the domain. The convergence order for a fixed mesh is lower than two for coarse grids given that at very low resolutions, the discrete solution becomes a step function for which the maximum convergence order achievable is one. For sufficiently high resolution, the grid captures well the flow features at the vortex center and we observe the second order convergence expected from the second order discretization methods implemented in Gerris. When applying AMR, we significantly reduce the numerical error for a constant resolution. Although the convergence order is similar to that of uniform grids, AMR starts showing a second order convergence for lower resolutions than a fixed discretization, which turns into smaller discretization errors for a fixed number of cells. It is also worthy noting that in the low resolution region, where the convergence order is lower than two, the global accuracy for AMR simulations is significantly improved compared to a uniform grid for a given number of cells (Fig. 6(b)). The main reason for that is that the computational effort is mainly focused at the vortex center, where the solution variation is abrupt, whereas the solution is significantly coarsened close to the domain boundaries.

For this particular example, where the analytical solution is known, it is also possible to investigate the local performance of the proposed error estimator. We note that local analyses are more challenging than global error estimations given that in addition to the total error we want to know how this error is distributed in the computational domain. In order to measure the local efficiency of the criterion to capture the real error, we measure the coefficient of determination, R^2, obtained from the correlation between the predicted error $\varepsilon_{\text{estimated}}$ with respect to the true error $\varepsilon_{\text{true}}$, which is defined as a difference between the numerical and analytical solution. Fig. 7(a) shows that the correlation between the error estimated and the true error for all tested resolutions is linear. In addition, the coefficient of determination is close to the ideal value ($R^2 = 1$). Fig. 7(b) shows that the proposed AMR method correctly quantifies the amount of error introduced by the numerical solution irrespective of the grid resolution. We therefore conclude that the proposed AMR method exhibits a good performance in order to minimize the total error in Lamb–Oseen like structures, giving also a good estimation of the local error distribution.

4.2.2. *Growth of random noise perturbations in a shear layer*

In this numerical test we investigate the capability of AMR to correctly capture the growth of small perturbations by a Kelvin–Helmholtz instability (KHI). KHI is defined as flow instability consequence of velocity difference between two parallel

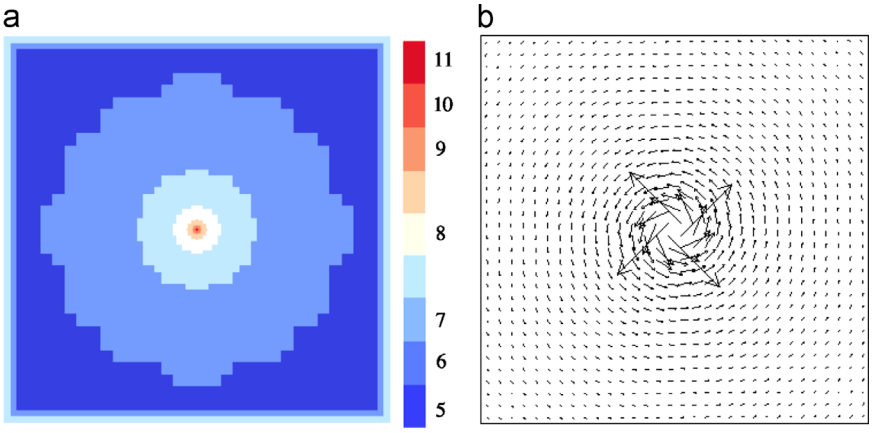

Fig. 5. Grid size distribution (a) and non-dimensional azimuthal velocity (b) snapshot. The color scale represents the level of refinement l defined as $2^l = L/\Delta x$. The computational effort is mainly focused on the solution where the variation is abrupt(center of the domain). The solution is significantly coarsened at the domain boundaries. (a) Grid distribution and (b) Lamb–Oseen velocity field.

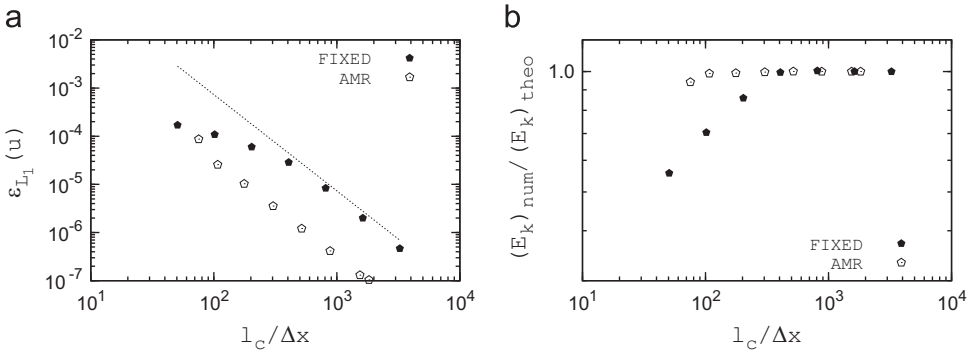

Fig. 6. Error convergence (a) and converged value (b) with a fixed and AMR mesh for the Lamb–Oseen vortex test case. For AMR simulations, the equivalent grid size is defined as $\Delta x = L/\sqrt{N_{\text{cells}}}$. (a) Error convergence of x component of velocity based on norm L_1 and (b) convergence of kinetic energy E_k on the circular region of radius $R_c/l_c = 100$.

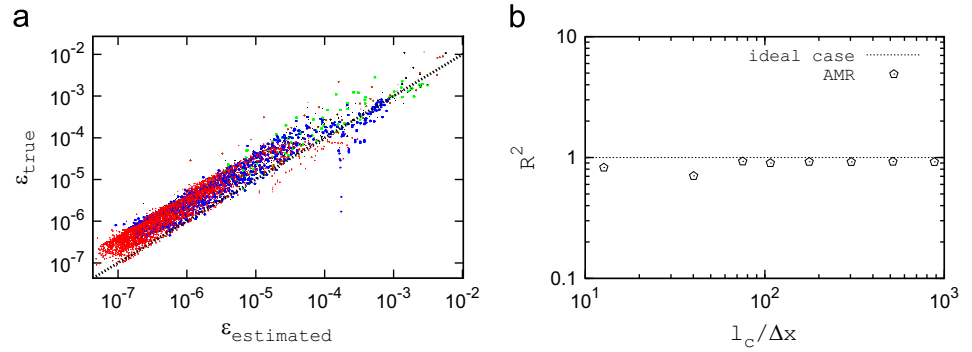

Fig. 7. Local error efficiency measurements for the Lamb–Oseen vortex test case. (a) Predicted error $\varepsilon_{\text{estimated}}$ versus true error $\varepsilon_{\text{true}}$ for all the resolutions tested and (b) coefficient of determination as a function of the grid resolution.

streams of different velocity and/or density. This mechanism is usually encountered in a relatively large number of process leading to the development of fully turbulent flows, such as the abrupt expansion in the diffuser region of the catalytic converter. In this paper we investigate the temporal evolution of small perturbations in a baseflow profile given by

$$U = \Delta U erf(y/\delta_c), \tag{14}$$

where δ_c is the boundary layer thickness. In this configuration, it is possible to solve for the linearized Navier–Stokes equations to find the theoretical growthrate as a function of the wavelength. The exact value used in this test case is obtained using the code developed by Otto et al. (2013) already tested and validated for the investigation of perturbation growth in shear layers. The theoretical growthrate c_i as a function of the wavelength α tends to the following asymptotic value when the Reynolds number is infinitely large

$$\alpha_m \delta_c = 0.5 \quad \frac{(\alpha c_i)_m \delta_c}{\Delta U} = 0.215737 \tag{15}$$

In order to reproduce these results, a simulation domain of size $[L_x/\delta_c, L_y/\delta_c] = [100, 300]$ is considered where ΔU and δ_c are taken as the characteristic velocity and length of the problem (Fig. 8(a)).

Random noise of low amplitude is initially imposed on top of the baseflow profile in order to excite all the possible wavelengths. The noise is introduced through a random source on the Navier–Stokes equation in the y direction modulated with a Gaussian distribution

$$S = \text{Rand}() e^{-y^2} \quad \frac{t\Delta U}{\delta_c} \leq 1. \tag{16}$$

The source is switched off for larger times.

A measure of the perturbation growth can be obtained by measuring the maximum amplitude of the vertical velocity V in time. In particular, Fig. 8(b) depicts the temporal evolution of the V component of the velocity integrated across the entire domain. After an initial transient state, the instability develops and generates well resolved structures that grow in time exponentially (Fig. 8(c)–(e)). The numerical growth-rate is obtained by fitting the perturbation growth in a time interval $t\Delta U/\delta_c = [30:50]$. The error is then computed by comparing the numerical and theoretical growthrate.

Fig. 9 depicts an example of the grid distribution typically generated. The grid is significantly refined at the velocity shear region where the velocity variations are important and it is coarsened gradually as variations become less important.

Fig. 10 shows the error in the growth-rate obtained for a uniform mesh and a non-uniform mesh adapted according to the Hessian error estimator in the vorticity field. As in the previous test case, the AMR grid provides more accurate than a fixed mesh for a given resolution (Fig. 10). AMR is able to start displaying second order convergence for lower resolutions given that it is able to concentrate the grid cells in those regions where the error is large. For coarse grids the convergence order is significantly degraded but in any case the AMR provides significantly more accurate solutions than a fixed grid for a fixed number of cells (Fig. 10(b)).

5. Validation of the subgrid pressure jump model

In this section we concentrate on the validation of the pressure jump model using the experiments presented by Benjamin (2003) and Benjamin et al. (2002), where only the expansion stage and

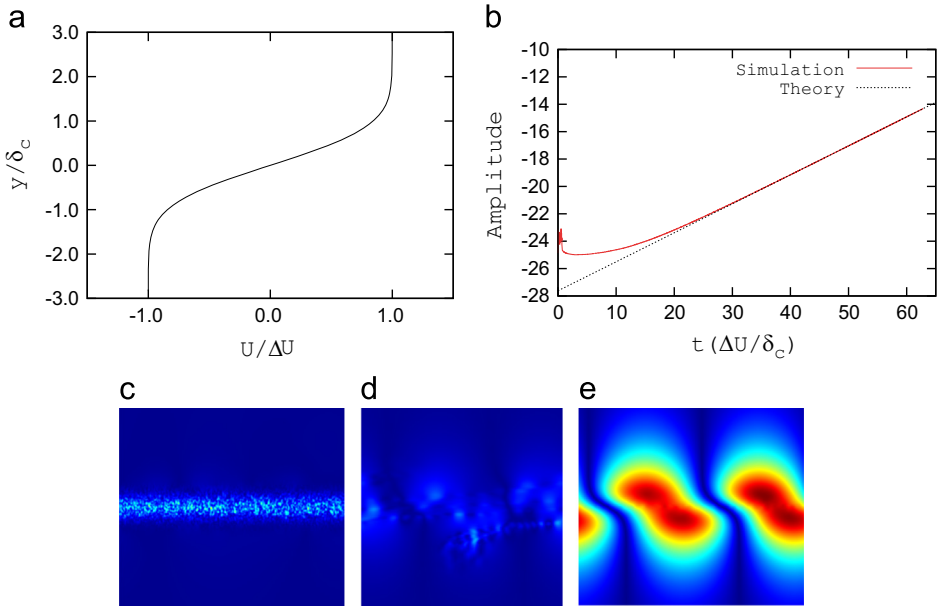

Fig. 8. Inviscid vortex test case. A random perturbation is imposed in a shear layer. The small perturbation initially imposed in the solution grows in time creating coherent structures corresponding to the most unstable mode for which a theoretical growthrate can be obtained. (a) Shear velocity profile, (b) temporal evolution of the amplitude disturbance integrated over the whole domain, (c) perturbed field at $t\Delta U/\delta_c = 0$, (d) perturbed field at $t\Delta U/\delta_c = 10$, and (e) perturbed field at $t\Delta U/\delta_c = 50$.

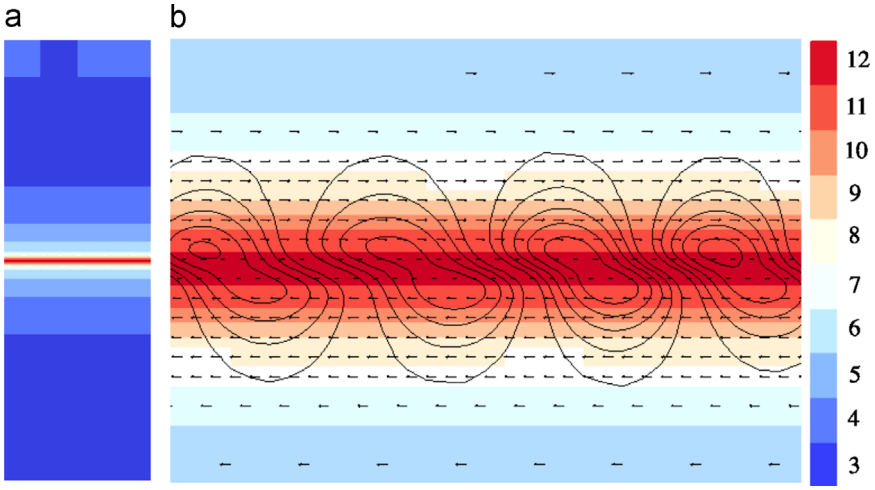

Fig. 9. Grid size distribution, velocity vectors and perturbation isolines (V) for the instability growth in a shear layer. Grid cells preferentially concentrate on the velocity shear layer region. (a) Grid distribution for the instability growth in a shear layer. The color scale represents the level of refinement l defined as $2^l = L/\Delta x$ and (b) zoom into the shear layer region.

the monolith substrate region are considered. These works were devoted to examine the flow distribution in automotive catalyst systems and to provide experimental data for verification of computational fluid dynamic simulations. The experimental set-up consists of a diffuser and a substrate. The diffuser is axially symmetric with a total angle 60° and length 61.5 mm. The inlet pipe diameter on which Reynolds number are based is 48 mm. The velocity profiles are measured 45 mm upstream of the diffuser throat. A tube is used to hold flow straighteners to achieve uniform flow. Two ceramic substrates of different lengths are used (152 mm and 102 mm respectively). Both substrates have a nominal cell density of 400 cspi made of square channels of 1 mm. The diameter of both substrates is 118 mm. Physical and geometrical properties of the experimental set-up are indicated in Table 2.

During the numerical investigations, we impose a uniform velocity profile at the inlet pipe. The walls of the system are treated as impermeable solid walls with no-slip boundary condition. For the outlet section, an outflow boundary condition is applied.

To evaluate the effect of geometry and mass flow rate on the flow distribution a non-uniformity index σ_V is defined using the variance of the velocity profile across a transversal section with respect to the averaged uniform velocity profile

$$\sigma_V = \frac{1}{\dot{m}} \int_A |U_i - U_e| \delta\dot{m}. \tag{17}$$

The non-uniformity index over the cross section of the substrate, ψ is defined as

$$\psi = \frac{\sigma_V}{U_e} \times 100. \tag{18}$$

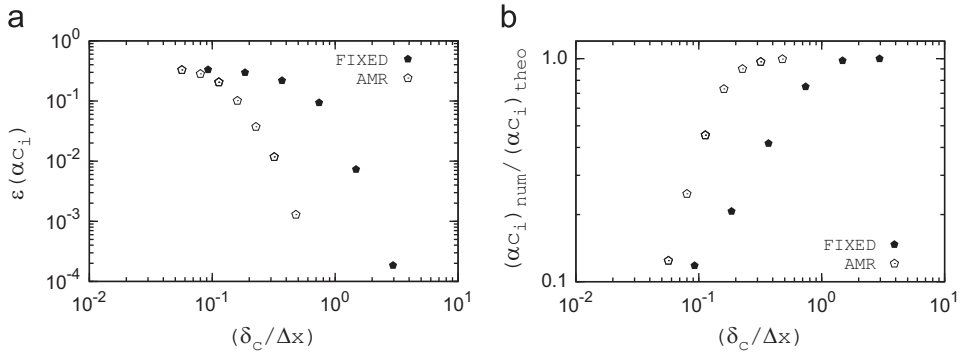

Fig. 10. Error convergence (a) and converged values (b) with a fixed and AMR mesh for the instability growth in a shear layer. For AMR, the equivalent grid size is obtained as $\Delta x = \sqrt{L_x \times L_y / N_{cells}}$. (a) Error convergence of αc_i and (b) converged value of αc_i.

Table 1
Simulation conditions used to test the subgrid model in Fig. 11.

Dimensions of the solution domain	
Pipe diameter (D_{in})	50 mm
Pipe throughout a monolith substrate length	75 mm
Catalyst diameter (D_{max})	100 mm
Catalyst length	100 mm
Reduced catalyst length in simulation	5 mm
Catalyst channel diameter	2 mm
Reynolds number at inlet pipe diameter (Re)	10,000
Inlet velocity profile	Uniform

Table 2
Simulation of experimental set-up.

Dimensions of the geometry	
Inlet pipe diameter	48 mm
Inlet pipe length	45 mm
Diffuser length	61.5 mm
Total diffuser angle	60°
Substrate diameter	118 mm
Substrate length	152–102 mm
Nominal substrate cell density	400 cpsi
Fluid properties	
Reynolds number at inlet pipe diameter (Re)	20,000–100,000
Inlet velocity profile	Uniform

This number increases as the flow becomes less uniformly distributed. For a perfectly distributed flow this number is zero.

Fig. 11 compares the vorticity fields obtained at various times. The flow patterns observed in the divergent region are similar to those observed by Benjamin (2003). The model is able to act as a porous wall that induces strong recirculation in the expansion region without the necessity to explicitly simulate the flow inside the monolith channels.

To validate the developed numerical tool we measure the non-uniformity index ψ as a function of the Reynolds number for the two monolith substrates tested in Benjamin et al. (2002). We start showing the convergence of the results for the monolith of length 152 mm for Re=20,000, 60,000, 80,000. As shown in Fig. 12 the model converges to a value relatively close to the experimental observations for all Reynolds numbers tested here. These results show that the AMR method allows us to obtain relatively accurate results with approximately 100 times less number of grid cells compared to a fixed mesh. The computational gain increases as the Reynolds increase. The reason for this effect is that the characteristic scales of the flow become smaller as the Reynolds increases and therefore, the efficiency of AMR increases for low resolution simulations.

Although the results provided by the model converge to a value relatively close to the experimental observations, we systematically observe that simulation results under-predict the experimental value for experimental conditions. To gain further insight about the source of this disagreement, we perform a systematic comparison of the non-uniformity index ψ for the two different substrates and as a function of the Reynolds number. Even though the simulation results are consistent with the experimental results, Fig. 13 shows that as the substrate length decreases, the accuracy of the model decreases too. This effect is important for short monoliths and high Reynolds numbers. This reveals a limitation of the pressure jump model: while the model assumes a fully developed laminar flow inside the channels, in real conditions there is certainly a transition region at the channels entrance in which the pressure lost is not correctly captured by the Hagen–Poiseuille pressure drop model. As expected, as the length of the channels increases it is less important the transition region on the total pressure drop and the model predictions become more accurate. The accuracy of the solution is also larger as the Reynolds number decreases. At any event, we can conclude that the accuracy of the numerical model is satisfactory given the significant amount of computational time save with respect to the cost that would be implicated in the simulation of the flow inside the channels.

A finer analysis about the source of discrepancy between numerical and experimental results shows that the thickness of the boundary layer at the inlet has an impact on the results obtained. For instance, Fig. 14 compares the experimental and numerical velocity radial distribution for Re=79,900 assuming that the velocity profile at the inlet pipe corresponds to

$$U(y) = U_0 \; erf\left(-\frac{y - R_{\text{inlet}}}{\delta}\right), \tag{19}$$

where δ is the boundary layer thickness at the inlet pipe. This parameter is important given that it controls the growthrate of the instability, which finally has an impact on the flow distribution downstream. The value of δ that provides the best fitting between simulation and experimental results is δ=5 mm. In this case, numerical results converge to the velocity profile given by Benjamin et al. (2002) as we reduce the tolerance of the AMR criterion (Table 3). Unfortunately, the boundary layer thickness is not explicitly given in Benjamin et al. (2002), which means that the numerical fitting of δ may hide errors introduced by the models used and also by the discretization method. In any case, the good fitting between numerical and experimental results is remarkable due to the low number of grid points used and the large Reynolds number tested.

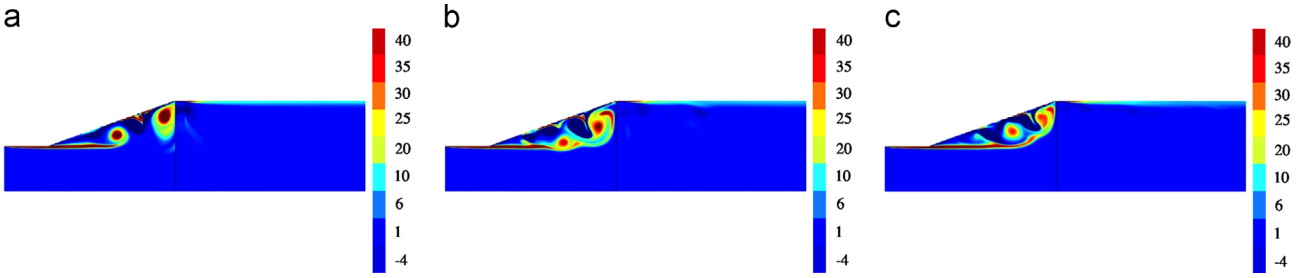

Fig. 11. Sequence of vorticity snapshots obtained with the pressure jump model. Diffuser and substrate properties are as shown in Table 1. The Reynolds number based on inlet pipe diameter is 10,000. The model is able to capture the effect of the substract on the flow upstream and to block the pass of vortices throughout the catalytic region as observed in the full simulation (Fig. 1) and experimental observations from Benjamin (2003).

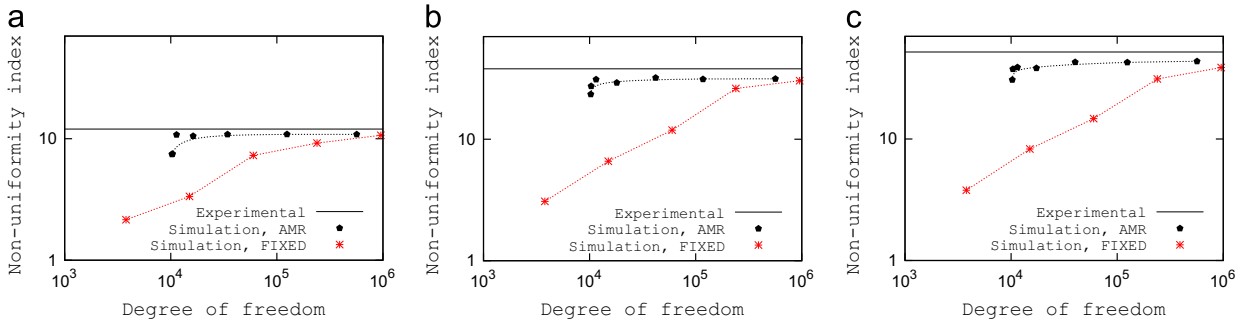

Fig. 12. Convergence tendencies of different grid designs at different regimes. (a) Re=20,000, (b) Re=60,000, and (c) Re=80,000.

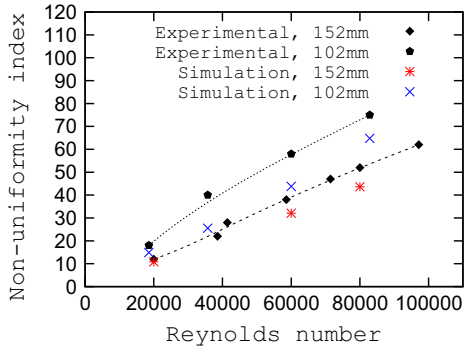

Fig. 13. Non-uniformity for different regimes and substrate lengths.

6. Numerical example

As an example of the capabilities of the developed models and numerical tools we present in this section the simulation results obtained for the simulation conditions included in Table 1 for using the whole geometry. The characteristic length of the system is chosen to be substrate diameter D_{max}.

All simulations were performed on a Dell Precision T5500 Westmere with a processor of Two Intel Xeon E5645 and total memory of 48 Go.

Fig. 15(a) depicts a sequence of snapshots of the resulting grid distribution obtained by vorticity based Hessian estimator. The grid is preferentially concentrated in the recirculation region, where most of the energy dissipation occurs (Fig. 15(b)) and where it is important to capture the flow features if one wants to correctly predict the flow distribution inside the different catalytic converter channels.

The combined use of the pressure drop model and AMR techniques significantly reduce the computational time (Fig. 16). We emphasize that this gain is expected to be even more significant in full three dimensional computations. The save in computational time is not at expenses of accuracy. As shown in Fig. 17 the velocity profiles at the medium plane obtained for the full numerical simulation and the simplified geometry match well. As it can be seen in Figs. 11 and 15(b) the reduced model captures remarkably well the influence of the substrate on the flow patterns upstream. The results are consistent with the flow patterns observed from the full simulation considering the substrate (Fig. 1) and also the flow patterns observed experimentally by Benjamin (2003).

7. Conclusion

In this paper we investigate a novel technique to couple the full solution of the Navier–Stokes equations in the divergent and convergent regions of a catalytic converter with a simplified physical model for the catalytic substrate.

The introduction of a new source term in the momentum equation allows us to capture the pressure drop induced by the catalytic substrate in the flow without the need of simulating the flow inside the catalytic channels. The model has been validated against the experimental results reported by Benjamin et al. (2002). The model still captures the influence of the substrate on the main flow features observed upstream saving a significant computational time.

In addition to the model for the catalytic substrate, specific multi-resolution techniques have been developed and validated against test cases related to the flow features observed in the diffuser region of catalytic converter systems. We conclude that by optimizing the grid distribution we can accelerate the simulation time by factor 10. This factor is expected to be larger for three dimensional computations.

To sum up, the coupling of models for the flow inside the catalytic substrate and the use of adaptive mesh refinement combined with efficient criteria for mesh adaptation produce optimum grid distributions that make possible to simulate complex flow problems involving different lengthscales in reasonable computational times. This work is currently being used as a solid

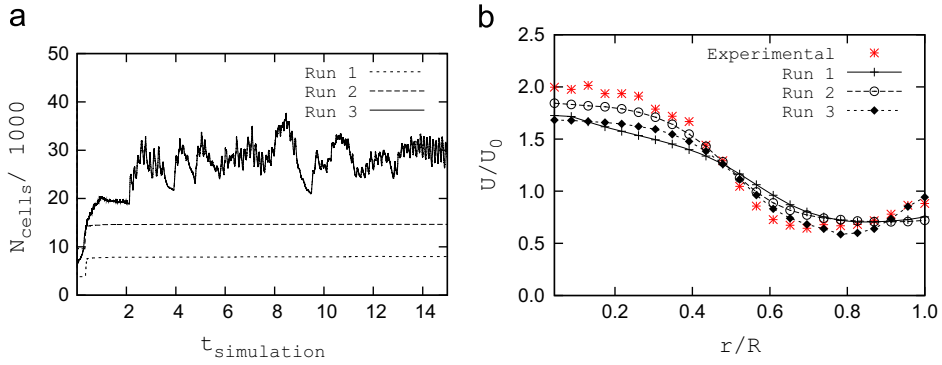

Fig. 14. Temporal evolution of the total grid points and convergence of the radial velocity profile at Re = 79,900 (based on inlet pipe diameter). The simulation results reproduce relatively well experimental results of Benjamin et al. (2002). (a) Number of total grid points as a function of the AMR tolerance (Table 3) and (b) velocity profiles for the three AMR tolerances contained in Table 3 (R represents the radius of the substrate).

Table 3
Simulations for radial velocity profile convergence.

Simulation	AMR tolerance η	Time averaged number of total grids
Run 1	$\eta < 0.7$	7970
Run 2	$\eta < 0.5$	14,651
Run 3	$\eta < 0.2$	28,799

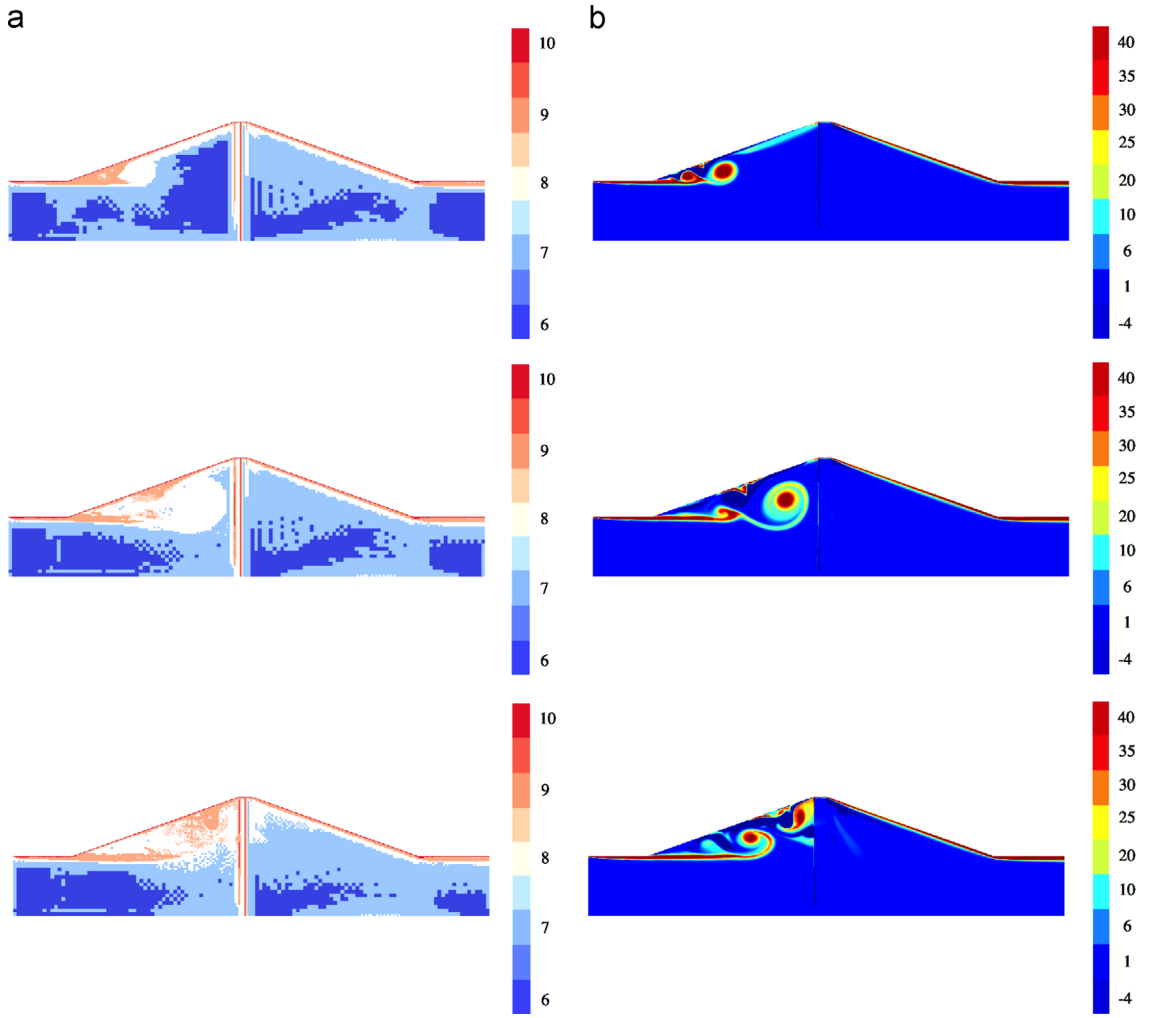

Fig. 15. Grid size distribution (a) and non-dimensional vorticity (b) snapshots. The color scale for grid distribution represents the level of refinement, l, so that $2^l = D_{max}/\Delta x$. The non-dimensionless vorticity is calculated as $\omega D_{max}/u_0$. The grid is preferentially concentrated in those regions where the vortical structures are present. (a) Grid distribution and (b) vorticity fields.

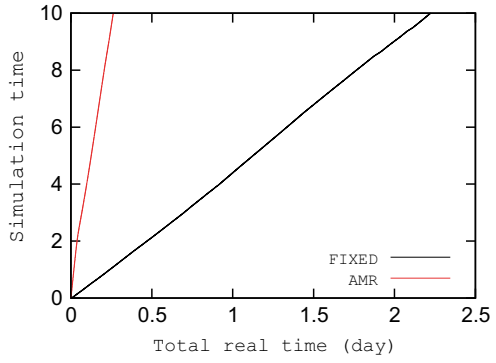

Fig. 16. Comparison of computational times for fixed and AMR mesh. The use of AMR techniques allows us to obtain results approximately 10 times faster compared to uniform fixed mesh for a given level of accuracy.

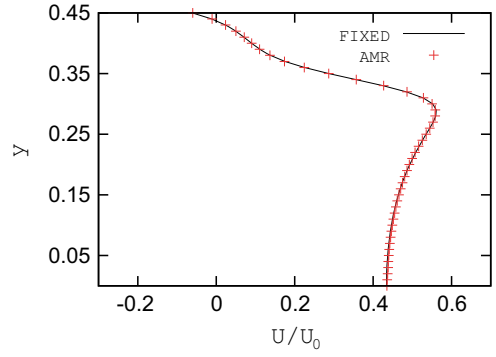

Fig. 17. Velocity profiles at the entrance of the substrate using a uniform grid and the AMR grid. Level of refinement employed for uniform grid is $l=9$ so that $D_{max}/\Delta x = 2^9$. Vorticity based Hessian estimator is used as AMR criterion.

platform in which to implement simplified chemical reaction models capable of providing a complete description of all the physical and chemical processes taking place inside the catalytic system such as diesel oxidation catalyst (DOC), NOx trap catalyst, and selective catalytic reduction (SCR) catalyst.

References

Agrawal, G., Kaisare, N., Pushpavanam, S., Ramanathan, K., 2012. Modelling the effect of flow mal-distribution on the performance of a catalytic converter. Chem. Eng. Sci. 71, 310–320.

Bella, G., Rocco, V., Maggiore, M., 1991. A study of inlet flow distortion effects on automotive catalytic converters. J. Eng. Gas Turbines Power 113.

Benjamin, S., 2003. Simulating the Performance of Automative Catalytic Converters. Technical Report, CAERT.

Benjamin, S., Liu, Z., Roberts, C., 2004. Automotive catalyst design for uniform conversion efficiency. Appl. Math. Model. 28 (6), 559–572.

Benjamin, S., Roberts, C., Wollin, J., 2002. A study of pulsating flow in automotive catalyst systems. Exp. Fluids 33, 629–639.

Bockhorn, H., Denev, J.A., Domingues, M., Falconi, C., Farge, M., Frohlich, J., Gomes, S., Kadoch, B., Molina, I., Roussel, O., et al., 2009. Numerical simulation of turbulent flows in complex geometries using the coherent vortex simulation approach based on orthonormal wavelet decomposition. In: Numerical Simulation of Turbulent Flows and Noise Generation. Springer, Berlin, pp. 175–200.

Chakravarthy, V., Conklin, J., Daw, C., Dazevedo, E., 2003. Multi-dimensional simulations of cold-start transients in a catalytic converter under steady inflow conditions. Appl. Catal. A-Gen 241 (1), 289–306.

Charpentier, J.C., 2005. Four main objectives for the future of chemical and process engineering mainly concerned by the science and technologies of new materials production. Chem. Eng. J. 107, 3–17.

Chatterjee, D., Deutschmann, O., Warnatz, J., 2002. Detailed surface reaction mechanism in a three-way catalyst. Faraday Discuss. 119, 371–384.

Davies, C., Carpenter, P.W., 2001. A novel velocity–vorticity formulation of the Navier–Stokes equations with applications to boundary layer disturbance evolution. J. Comput. Phys. 172, 119–165.

Depcik, C., Loya, S., 2012. Dynamically incompressible flow. Advanced Methods for Practical Applications in Fluid Mechanics. In: S. Jones (Ed.), InTech, New York.

Forrester, S.E., Evans, G.M., 1997. Computational modelling study of the hydrodynamics in a sudden expansion–tapered contraction reactor geometry. Chem. Eng. Sci. 52, 3773–3785.

Fuster, D., Agbaglah, G., Josserand, C., Popinet, S., Zaleski, S., 2009a. Numerical simulation of droplets, bubbles and waves: state of the art. Fluid Dyn. Res. 41, 065001.

Fuster, D., Bagué, A., Boeck, T., Le Moyne, L., Leboissetier, A., Popinet, S., Ray, P., Scardovelli, R., Zaleski, S., 2009b. Simulation of primary atomization with an octree adaptive mesh refinement and VOF method. Int. J. Mult. Flow 35, 550–565.

Fuster, D., Matas, J.P., Marty, S., Popinet, S., Hoepffner, J., Cartellier, A., Zaleski, S., 2013. Instability regimes in the primary breakup region of planar coflowing sheets. J. Fluid Mech. 736, 150–176.

Gao, X., Groth, C.P.T., 2006. A parallel adaptive mesh refinement algorithm for predicting turbulent non-premixed combusting flows. Int. J. Comput. Fluid Dyn. 20, 349–357.

Gao, X., Groth, C.P.T., 2010. A parallel solution—adaptive method for three-dimensional turbulent non-premixed combusting flows. J. Comput. Phys. 229, 3250–3275.

Guojiang, W., Song, T., 2005. Cfd simulation of the effect of upstream flow distribution on the light-off performance of a catalytic converter. Energy Convers. Manage. 46, 2010–2031.

Hauke, G., Fuster, D., Doweidar, M., 2008. Variational multiscale a-posteriori error estimation for multi-dimensional transport problems. Comput. Methods Appl. Mech. Eng. 197, 2701–2718.

Heck, R.M., Gulati, S., Farrauto, R.J., 2001. The application of monoliths for gas phase catalytic reactions. Chem. Eng. J. 82, 149–156.

Holmgren, A., Gronstedt, T., Andersson, B., 1997. Improved flow distribution in automotive monolithic converters. React. Kinet. Catal. L. 60 (2), 363–371.

Karvounis, E., Assanis, D.N., 1993. The effect of inlet flow distribution on catalytic conversion efficiency. Int. J. Heat Mass Transf. 36, 1495–1504.

Lai, M., Lee, T., Kim, J., Cheng, C., Li, P., Chui, G., 1992. Numerical and experimental characterizations of automotive catalytic converter internal flows. J. Fluid Struct. 6 (4), 451–470.

Meunier, P., Villermaux, E., 2003. How vortices mix. J. Fluid Mech. 476, 213–222.

Nazarov, M., Hoffman, J., 2013. Residual-based artificial viscosity for simulation of turbulent compressible flow using adaptive finite element methods. Int. J. Numer. Meth. Fluids 71, 339–357.

Neve, R.S., 1993. Computational fluid dynamics analysis of diffuser performance in gas-powered jet pumps. Int. J. Heat Fluid Flow 14, 401–407.

Nien, T., Mmbaga, J.P., Hayes, R.E., Votsmeier, M., 2013. Hierarchical multi-scale model reduction in the simulation of catalytic converters. Chem. Eng. Sci. 93, 362–375.

Olshanskii, M.A., Rebholz, L.G., 2010. Velocity–vorticity–helicity formulation and a solver for the Navier–Stokes equations. J. Comput. Phys. 229, 4291–4303.

Otto, T., Rossi, M., Boeck, T., 2013. Viscous instability of a sheared liquid–gas interface: dependence on fluid properties and basic velocity profile. Phys. Fluids 25, 032103.

Pachauri, R.K., Reisinger, A., 2007. Climate Change 2007: synthesis Report. Contribution of Working Groups i, ii and iii to the Fourth Assessment Report of the Intergovernmental Panel on Climate Change. IPCC 1.

Pontikakis, G.N., Konstantas, G.S., Stamatelos, A.M., 2004. Three-way catalytic converter modeling as a modern engineering design tool. J. Eng. Gas Turbines Power 126, 906–923.

Popinet, S., 2003. Gerris: a tree-based adaptive solver for the incompressible Euler equations in complex geometries. J. Comput. Phys. 190, 572–600.

Popinet, S., 2009. An accurate adaptive solver for surface-tension-driven interfacial flows. J. Comput. Phys. 228, 5838–5866.

Shuja, S.Z., Habib, M.A., 1996. Fluid flow and heat transfer characteristics in axisymmetric annular diffusers. Comput. Fluids 25, 133–150.

Siemund, S., Leclerc, J.P., Schweich, D., Prigent, M., Castagna, F., 1996. Three-way monolithic converter: simulations versus experiments. Chem. Eng. Sci. 51, 3709–3720.

Skelland, A., 1974. Diffusional Mass Transfer. Wiley, New York.

Tischer, S., Correa, C., Deutschmann, O., 2001. Transient three-dimensional simulations of a catalytic combustion monolith using detailed models for heterogeneous and homogeneous reactions and transport phenomena. Catal. Today 69, 57–62.

Tischer, S., Deutschmann, O., 2005. Recent advances in numerical modeling of catalytic monolith reactors. Catal. Today 105, 407–413.

Ubertini, S., Desideri, U., 2000. Experimental performance analysis of an annular diffuser with and without struts. Exp. Therm. Fluid Sci. 22, 183–195.